

SAGA: Selective Adaptive Gating for Efficient and Expressive Linear Attention

Yuan Cao, Dong Wang

Institute of Information Science, Beijing Jiaotong University
No.3 Shangyuan Village, Xizhimenwai, Haidian District, Beijing, China, 100044

Abstract

While Transformer architecture excel at modeling long-range dependencies—contributing to its widespread adoption in vision tasks—the quadratic complexity of softmax-based attention mechanisms imposes a major bottleneck, particularly when processing high-resolution images. Linear attention presents a promising alternative by reformulating the attention computation from $(QK)V$ to $Q(KV)$, thereby reducing the complexity from $\mathcal{O}(N^2)$ to $\mathcal{O}(N)$ while preserving the global receptive field. However, most existing methods compress historical key-value (KV) information uniformly, which can lead to feature redundancy and the loss of directional alignment with the query (Q). This uniform compression results in low-rank KV feature maps, contributing to a performance gap compared to softmax attention. To mitigate this limitation, we propose **Selective Adaptive Gating for Efficient and Expressive Linear Attention (SAGA)**, which introduces input-adaptive learnable gates to selectively modulate information aggregation into the KV feature map. These gates enhance semantic diversity and alleviate the low-rank constraint inherent in conventional linear attention. Additionally, we propose an efficient Hadamard-product decomposition method for gate computation, which introduces no additional memory overhead. Experiments demonstrate that SAGA achieves a $1.76\times$ improvement in throughput and a $2.69\times$ reduction in peak GPU memory compared to PVT-T at a resolution of 1280×1280 . Moreover, it improves top-1 accuracy by up to 4.4% on the ImageNet dataset, demonstrating both computational efficiency and model effectiveness.

Introduction

Introduction

In recent years, the Vision Transformer (ViT) (Dosovitskiy et al., 2020) has attracted considerable attention for its exceptional long-range modeling capacity. By explicitly computing pairwise token affinities across the entire input sequence, ViT establishes global semantic relationships, delivering robust performance across diverse visual tasks (Yuan et al., 2021; Xie et al., 2021; Fang et al., 2023).

Copyright © 2025, Association for the Advancement of Artificial Intelligence (www.aaai.org). All rights reserved.

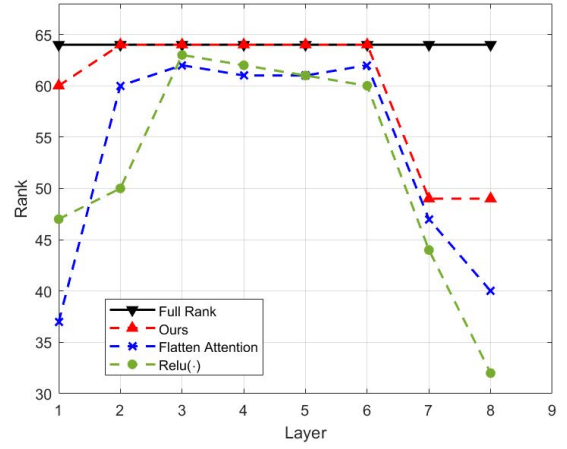


Figure 1: Comparison of rank curves between $Relu(\cdot)$, Flatten Attention and our SAGA.

However, the quadratic complexity of its softmax attention mechanism renders ViT computationally intensive for high-resolution imagery, limiting its applicability in real-world scenarios (Meng et al., 2025a; Xie et al., 2024). To address this, recent efforts have focused on accelerating attention computation. For instance, PVT (Wang et al., 2021) employs sparse attention by downsampling key-value pairs to reduce computational overhead, while the Swin Transformer (Liu et al., 2021b) restricts attention to local windows through local attention. Although these strategies effectively lower computational overhead, they inherently restrict the model’s receptive field, sacrificing global contextual modeling and often resulting in measurable performance degradation.

To reconcile model efficiency with the preservation of a global receptive field, linear attention (Katharopoulos et al., 2020) has been proposed as a computationally efficient alternative to softmax-based attention. By employing kernel function mapping and reordering the attention computation from $(QK)V$ to $Q(KV)$, linear attention reduces the computational complexity from $\mathcal{O}(N^2d)$ to $\mathcal{O}(Nd^2)$, where N denotes the number of tokens and d denotes the embedding dimension. Crucially, this reformulation yields a fixed-size key-value (KV) feature map of shape $d_k \times d_v$, independent

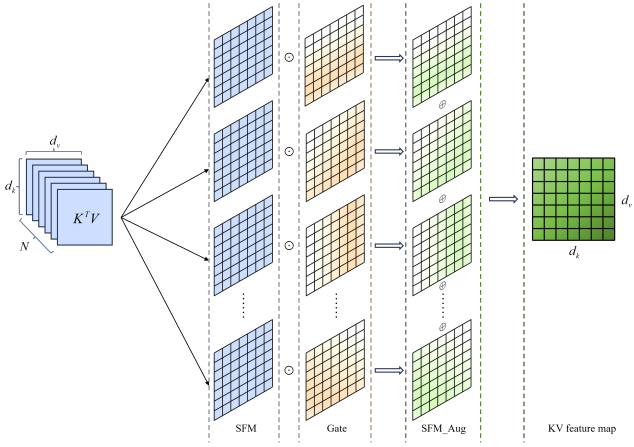


Figure 2: Illustration of KVGate module. The process of $K^T V$ essentially involves the summation of N matrices of size $d_k \times d_v$, which can be interpreted as the information fusion of the SFM corresponding to N tokens. We introduced a gate layer for each SFM to refine the information flow entering KV feature map.

of the sequence length N . This compact representation functions as a **global semantic repository**, effectively encoding long-range dependencies and enabling query Q to dynamically retrieve relevant contextual information (Shen et al., 2021).

However, linear attention typically suffers a notable performance degradation compared to softmax attention. To investigate the root cause of this gap, we conduct a systematic analysis of the KV feature map—the core component responsible for encoding global contextual information. We characterize the feature diversity of the semantic repository by analyzing the rank of the KV feature map. Fig. 1 presents the rank evolution of several linear attention variants within the PVT-T architecture. In all cases, the curves remain significantly below the full-rank upper bound, indicating substantial feature redundancy in the compressed global representation. This low-rank structure limits the expressive capacity of the query Q to effectively retrieve and attend to diverse contextual patterns. Therefore, enhancing the rank of the KV feature map is essential to improving global context modeling and overall model performance.

To address the low-rank bottleneck in the KV feature map, we first analyze its fundamental causes. As illustrated in Fig. 2, the KV feature map is constructed by aggregating N intermediate state feature maps (SFM), where each SFM corresponds to a rank-1 matrix $k_i^T v_i$ for the i -th token. This construction amounts to an undifferentiated, fixed-size compression of all token-wise information, thereby erasing directional cues critical to the query. Consequently, the resulting KV feature map fails to establish discriminative affinities between the current query and historical key-value pairs, which leads to the attenuation of relevant contextual signals and the persistence of irrelevant information. We therefore identify the primary source of the low-rank structure as the indiscriminate aggregation of key-value contri-

butions, which introduces significant redundancy and limits representational capacity.

Building upon this analysis and inspired by LSTM/GRU (Graves and Graves, 2012; Chung et al., 2014), we propose the KVGate module, which assigns an input-adaptive gating matrix to each token-specific intermediate SFM. As illustrated in Fig. 2, this mechanism adaptively modulates each SFM’s contribution to the KV feature map, selectively enhancing relevant features while suppressing irrelevant components. Mathematically, this non-linear re-weighting yields a sharp increase in matrix rank, substantially enriching the feature diversity of the semantic repository.

However, directly integrating gating mechanisms into linear attention necessitates computing and storing both the intermediate SFM and the corresponding gating matrices for all N tokens, resulting in substantial memory overhead. To mitigate this burden, we propose a Hadamard product decomposition method that factorizes the gating matrices and applies it to the key (K) and value (V) matrices. This formulation eliminates the need to store all intermediate SFMs and gating matrices, reducing memory complexity while fully exploiting the parallelization capabilities of modern GPUs for accelerated computation.

The main contributions of this work are summarized as follows:

- We propose **KVGate**, a novel gating module for linear attention that selectively modulates the contribution of each intermediate SFM to the KV feature map through input-adaptive gating mechanisms. By amplifying relevant information and suppressing irrelevant ones, KVGate enhances the representational capacity of linear attention while preserving computational efficiency.
- To address the memory overhead associated with storing intermediate SFMs and gating tensors across all tokens, we introduce a **Hadamard-product decomposition** strategy. This approach factorizes the gating matrices and applies it to the key (K) and value (V) matrices, eliminating the need to store full gating matrices and intermediate SFM. It significantly reduces memory consumption and is highly amenable to GPU parallelization.
- We integrate KVGate into several state-of-the-art Vision Transformer architectures and evaluate it on image classification, semantic segmentation and object detection. On ImageNet-1K, our method improves top-1 accuracy by up to 4.4% over baseline models and realizes a throughput increase of $1.76\times$ and a reduction of $2.69\times$ in Peak GPU Memory at a resolution of 1280×1208 under the PVT-T framework. These results validate the effectiveness and efficiency of KVGate in real-world vision applications.

Related Work

Following the rise of Transformer and softmax attention in the field of NLP, the vision community has witnessed a surge of interest (Dosovitskiy et al., 2020; Carion et al., 2020; Xie et al., 2021; Liang et al., 2021) in adapting self-attention mechanisms to computer-vision tasks. However,

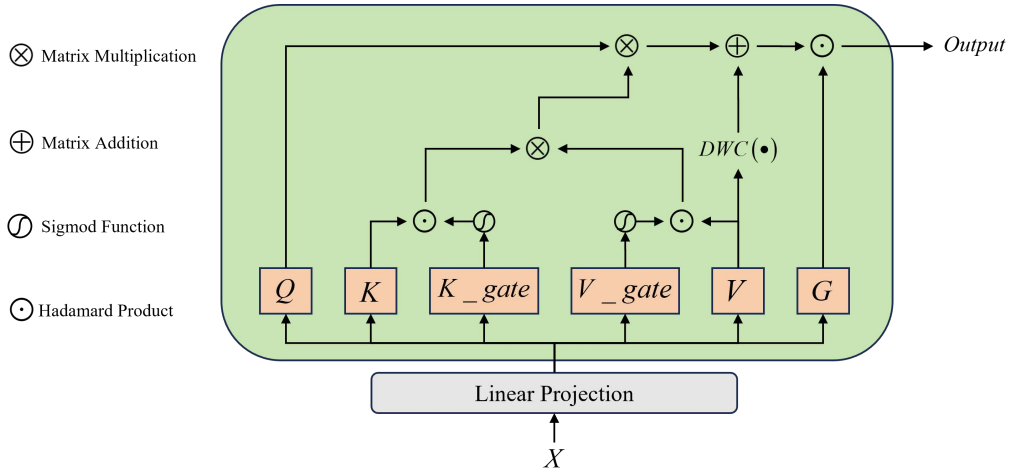


Figure 3: The overall architecture of SAGA.

the quadratic complexity of self-attention incurs prohibitive training costs, thereby hindering the broader deployment of ViT-based architectures in resource-constrained scenarios. To tackle this problem, a variety of efficient variants have been proposed, such as sparse attention (Wang et al., 2021; Xia et al., 2022), local attention (Liu et al., 2021b; Hassani et al., 2023) and hybrid model (Dai et al., 2021; Yang et al., 2022; Hou et al., 2024). While these methods improve efficiency, they compromise long-range dependencies and fail to address the quadratic complexity issue. Linear attention fundamentally addresses the quadratic complexity issue and reduces the model’s complexity from $\mathcal{O}(N^2)$ to $\mathcal{O}(N)$. Some existing work replaces softmax attention with normalized attention scores. For example, Hydra attention (Qin et al., 2022) employs a cosine kernel instead of the softmax operator, Flatten attention (Han et al., 2023) uses power operations to focus attention scores and obtain sharp attention distributions, and PolaFormer (Meng et al., 2025b) explicitly models the interactions between query-key pairs with the same and opposite signs, fully considering the impact of negative values in query-key pairs. Simultaneously, other works abandon the normalized attention form and start from the intermediate SFM to emphasize the contributions of different SFMs to the output. RetNet (Sun et al., 2023) introduces a distance-dependent decay matrix to attenuate SFMs that are farther apart, while GLA (Yang et al., 2023) incorporates an input-dependent decay matrix to adaptively attenuate SFMs.

Preliminary

In this section, we begin by reviewing the standard softmax attention mechanism, followed by an exposition of both normalized and unnormalized variants of linear attention. For clarity of presentation, we focus on the single-head formulation.

Softmax Attention. Within a standard attention head, the input $x \in \mathbb{R}^{N \times d}$ is a sequence with token length N and dimension d . Through linear mappings, x is projected into

the $Q = \{q_t\}_{t=1}^N$, $K = \{k_t\}_{t=1}^N$, and $V = \{v_t\}_{t=1}^N$. The output $O = \{o_t\}_{t=1}^N$ of softmax attention can be expressed as follows:

$$o_t = \frac{\sum_i^N \exp\left(q_t k_i^T / \sqrt{d}\right)}{\sum_j^N \exp\left(q_t k_j^T / \sqrt{d}\right)} v_i \quad (1)$$

Through softmax attention, each token at a given position can obtain information from tokens at other positions. However, this approach incurs a complexity of $\mathcal{O}(N^2 d)$.

Normalized Linear Attention. To enhance the computational efficiency of self-attention mechanisms, linear attention replaces the softmax attention’s $\exp(q_t k_i^T)$ with $\phi(q_t) \phi(k_i)^T$ and leverages the associative property of matrix multiplication to change the computation order from $(QK^T)V$ to $Q(K^T V)$, thereby reducing the complexity to $\mathcal{O}(Nd^2)$. Normalized linear attention can be expressed as follows:

$$o_t = \frac{\sum_i^N \phi(q_t) \phi(k_i)^T v_i}{\sum_j^N \phi(q_t) \phi(k_j)^T} = \frac{\phi(q_t) \sum_i^N \phi(k_i)^T v_i}{\phi(q_t) \sum_j^N \phi(k_j)^T} \quad (2)$$

Where $\phi(\cdot)$ is a kernel function mapping that enables normalized linear attention to approximate softmax attention.

Unnormalized Linear Attention. In NLP field, (Sun et al., 2023) found that linear attention using an identity mapping kernel without normalization performs well in practice. Therefore, linear attention can be simplified as follows:

$$S_t = S_{t-1} + k_t^T v_t, \quad o_t = q_t S_t \quad (3)$$

Where $S_t = \sum_{i=1}^t k_i^T v_i \in \mathbb{R}^{d_k \times d_v}$ represents the historical state, which is used to store the historical information of tokens.

Method

KV Gate. Starting from Eq. (3), it is crucial to clarify the distinctions between vision and NLP. In NLP, a causal con-

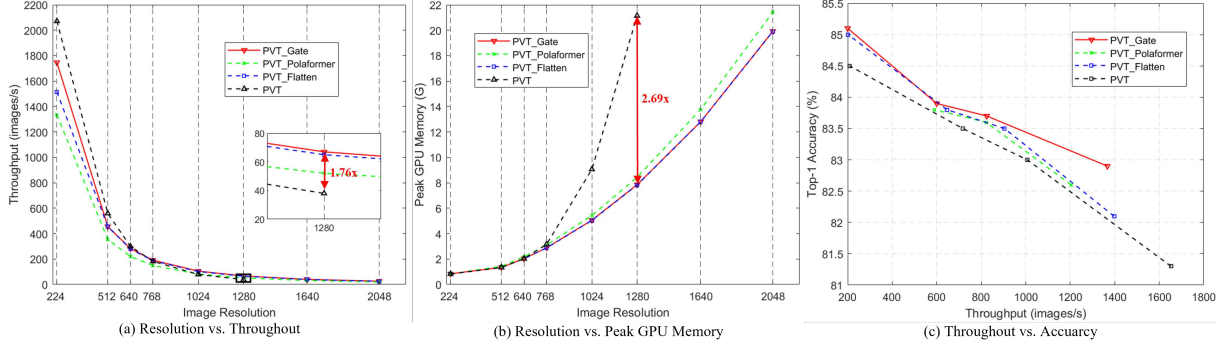


Figure 4: Efficiency analysis with (a) Resolution vs. Throughput, (b) Resolution vs. Peak GPU Memory and (c) Throughput vs. Accuracy. (a) and (b) are measured on a single 4090 GPU with batch size 16. (c) is measured with batch size 256.

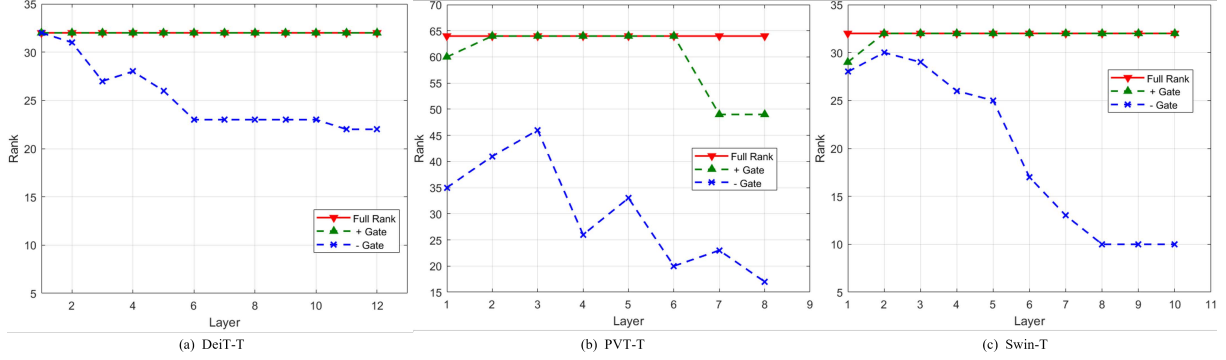


Figure 5: The rank changes of KV feature maps for DeiT-T, PVT-T, and Swin-T before and after adding the KVGate module.

straint exists, implying that each position can only attend to tokens preceding it. Consequently, the summation in Eq. (3) extends only up to the current position t . In contrast, visual data lacks such causal constraints, permitting each position to attend to tokens at all positions. Eq. (3) can thus be rewritten as follows:

$$o_t = q_t S = q_t \sum_{i=1}^N k_i^T v_i \quad (4)$$

Where N denotes the number of tokens in an image. $k_i^T v_i$ represents the intermediate SFM corresponding to the i -th token.

When applying linear attention to visual data, each query q_t attends to a fixed-size KV feature map $S \in \mathbb{R}^{d_k \times d_v}$, from which different queries extract features. Consequently, we can regard S as a **global semantic repository** comprising d_k global semantic vectors, each with a dimension of d_v .

When the intermediate SFM are linearly summed to obtain S , this approach prevents the S from effectively distinguishing the differences and connections between key-value pairs. As a result, it fails to highlight relevant information and discard irrelevant information. This issue is specifically manifested in the low-rank nature of the S , which introduces redundancy in the semantic repository.

As shown in Fig. 2, inspired by LSTM and GLA, we intro-

duce an input-adaptive gate G for the SFM to finely control the information flow into S . Unlike LSTM/GLA, the G we propose is not applied to S_t in Eq. 3 as a forget gate for the history state, but rather to the $k_t^T v_t$ to dynamically modulate the information flow of the intermediate SFM into the S . In visual data, this method can simultaneously modulate the information flow of the SFM corresponding to all tokens, thereby endowing the S with stronger feature representation capabilities. This can be interpreted as a weighted sum of all SFMs:

$$o_t = q_t S_g = q_t \sum_{i=1}^N G_i \odot k_i^T v_i \quad (5)$$

Where $G_i \in (0, 1)^{d_k \times d_v}$ is input-adaptive gating matrix.

Hadamard-product Decomposition. Traditional linear attention computes S directly via $K^T V$, leveraging the high-performance implementation of the code framework to occupy fewer resources. However, Eq. (5) faces a thorny issue in application: the presence of G_i necessitates the computation of the intermediate SFM for each of the N tokens. This implies the need to maintain a matrix of size $2 \times N \times d_k \times d_v$, including both the SFM and G_t , thereby causing a substantial increase in storage resources.

To reduce memory consumption, we derive a decomposition method of the Hadamard-product:

Property. Let $A, C \in \mathbb{R}^{d \times 1}$ and let $B, D \in \mathbb{R}^{1 \times d}$, we have:

$$AB \odot CD = (A \odot C)(B \odot D) \quad (6)$$

Proof.

Left-hand side of the equation:

- AB is a $d \times d$ matrix, whose elements are $A_i B_j$.
- CD is a $d \times d$ matrix, whose elements are $C_i D_j$.
- The result of the Hadamard-product is $(A_i B_j)(C_i D_j) = A_i B_j C_i D_j$.

Right-hand side of the equation:

- $(A \odot C)$ is a $d \times 1$ matrix, whose elements are $A_i C_i$.
- $(B \odot D)$ is a $1 \times d$ matrix, whose elements are $B_j D_j$.
- The product of the matrix multiplication results in a $d \times d$ matrix, whose elements are $(A_i C_i)(B_j D_j) = A_i B_j C_i D_j$.

The elements on both sides of the equation are equal, the equation holds true. The detailed derivation process can be found in the appendix.

Combining Eq.(6), we decompose G_i into $\alpha_i^T \beta_i$, where $\alpha_i \in (0, 1)^{1 \times d_k}$ and $\beta_i \in (0, 1)^{1 \times d_v}$:

$$\begin{aligned} o_t &= q_t \sum_{i=1}^N \alpha_i^T \beta_i \odot k_i^T v_i \\ &= q_t \sum_{i=1}^N (\alpha_i^T \odot k_i^T) (\beta_i \odot v_i) \end{aligned} \quad (7)$$

The matrix form is as follows:

$$O = Q \left[(K \odot A)^T (V \odot B) \right] \quad (8)$$

where $A \in (0, 1)^{N \times d_k}$ and $B \in (0, 1)^{N \times d_v}$.

It is necessary to additionally maintain A and B , which requires storage space of $N \times (d_k + d_v) < 2 \times N \times d_k \times d_v$.

The generation methods for A and B are identical to those for Q , K and V :

$$A = \text{sigmoid}(XW_A), B = \text{sigmoid}(XW_B) \quad (9)$$

Therefore, as depicted in Fig. 3, the final form of the linear attention proposed in this paper can be expressed as follows, where $G = XW_g \in \mathbb{R}^{N \times d}$ is introduced to further enhance nonlinearity (Sun et al., 2023)), $K_gate = A$ and $V_gate = B$:

$$\begin{aligned} \tilde{K} &= K \odot K_gate, \quad \tilde{V} = V \odot V_gate \\ O &= \left[Q \left[\tilde{K} \tilde{V} \right] + DWC(V) \right] \odot G \end{aligned} \quad (10)$$

The introduction of this gating mechanism enables the KV feature map to distinguish the importance information and remove noise from the intermediate SFM. From a mathematical perspective, this nonlinear mapping based on the Hadamard-product can significantly increase the rank of the KV feature map, thereby enriching the feature diversity of the semantic repository.

Method	Reso	Params	FLOPs	Tp.	Acc(%)
PlainMamba-L1	224 ²	7M	3.0G	995	77.9
ViG-S	224 ²	23M	3.5G	1886	81.7
VRWKV-S	224 ²	24M	4.6G	1724	80.1
LocalVMamba-T	224 ²	26M	5.7G	330	82.7
VMamba-T	224 ²	31M	4.9G	1161	82.5
ConvNeXt-S	224 ²	50M	8.7G	905	83.1
gMLP-B	224 ²	73M	15.8G	647	81.6
PVT-T-PolaFormer	224 ²	12M	2.0G	1733	78.8
PVT-S-PolaFormer	224 ²	21M	4.0G	949	81.9
PVTv2-b0-PolaFormer	224 ²	3.4M	0.6G	-	72.3
PVTv2-b1-PolaFormer	224 ²	13M	2.2G	-	80.2
Swin-S-PolaFormer	224 ²	50M	8.7G	822	83.6
Swin-B-PolaFormer	224 ²	88M	15.4G	590	83.8
DeiT-T	224 ²	5.7M	1.2G	5761	72.2
DeiT-T-SAGA	224 ²	7.0M	1.4G	4990	75.5 (+3.3)
PVT-T	224 ²	13.2M	1.9G	2995	75.1
PVT-T-SAGA	224 ²	14.5M	2.4G	2205	79.5 (+4.4)
PVT-S	224 ²	24.5M	3.8G	1873	79.8
PVT-S-SAGA	224 ²	26.1M	4.8G	1216	81.8 (+2.0)
PVTv2-b0	224 ²	3.7M	0.6G	4585	70.5
PVTv2-b0-SAGA	224 ²	4.2M	0.7G	3616	73.1 (+2.6)
PVTv2-b1	224 ²	13M	2.1G	2484	78.7
PVTv2-b1-SAGA	224 ²	15M	2.6G	1806	80.6 (+1.9)
Swin-T	224 ²	29M	4.5G	1511	81.3
Swin-T-SAGA	224 ²	32M	5.3G	1367	83.0 (+1.7)
Swin-S	224 ²	50M	8.7G	915	83.0
Swin-S-SAGA	224 ²	60M	10.6G	825	83.7 (+0.7)
Swin-B	224 ²	88M	15.4G	661	83.5
Swin-B-SAGA	224 ²	105M	18.8G	600	83.8 (+0.3)
Swin-B	384 ²	88M	47.0G	210	84.5
Swin-B-SAGA	384 ²	105M	55.3G	200	84.7 (+0.2)

Table 1: Comparison of image classification results on the ImageNet-1K dataset. Tp. (images/s) is measured on a single 4090 GPU with batch size 256.

Complexity Analysis. Let d denote the number of channels, and k denote the size of the convolution kernel. The computational cost of calculating Q , K , V , K_gate , V_gate , G and outputs projections is $7Nd^2$. The Hadamard-product of (K, K_gate) and (V, V_gate) has a computational cost of $2Nd$. The attention computation for (Q, K, V) requires a computational cost of $2Nd^2$. The convolution operation requires k^2Nd . The computational cost required for output augment G is Nd . In summary, the total complexity of SAGA is given by Eq.(11), and it exhibits linear complexity with respect to N .

$$\Theta = 9Nd^2 + k^2Nd + 3Nd \quad (11)$$

Experiment

We validated the effectiveness of the proposed model on the tasks of image classification, semantic segmentation and object detection using the ImageNet-1K (Deng et al., 2009), ADE20K (Zhou et al., 2019) and COCO datasets (Lin et al., 2014)). We first replaced softmax attention with the proposed SAGA and trained the models from scratch on ImageNet-1K. Subsequently, using the pre-trained models as backbones, we fine-tuned image segmentation models on ADE20K and object detection models on COCO. All models are trained and fine-tuned on 8 NVIDIA RTX 3090 GPUs

Method	Sch.	Type	AP^b	Detection and Instance Segmentation					Semantic Seg	
				AP_{50}^b	AP_{75}^b	AP^m	AP_{50}^m	AP_{75}^m	Type	mIoU
PVT-T	1×	R	36.7	-	-	-	-	-	S	36.57
	1×	M	36.7	59.2	39.3	35.1	56.7	37.3		
PVT-T-Flatten	1×	R	-	-	-	-	-	-	S	37.21
	1×	M	38.2	61.6	41.9	37.0	57.6	39		
PVT-T-PolaFormer	1×	R	39.5	60.1	42.1	-	-	-	S	38.30
	1×	M	40.4	62.4	43.9	37.4	59.4	40.3		
PVT-T-SAGA	1×	R	39.9(+3.2)	60.4	42.5	-	-	-	S	41.03(+4.46)
	1×	M	40.6(+3.9)	62.9(+3.7)	44.4(+5.1)	38.0(+2.9)	59.9(+3.2)	40.7(+3.4)		
Swin-T	1×	M	43.7	66.6	47.7	39.8	63.3	42.7	U	44.51
	3×	M	46.0	68.1	50.3	41.6	65.1	44.9		
	3×	C	50.4	69.2	54.7	43.7	66.6	47.3		
Swin-T-Flatten	1×	M	44.3	67.3	48.5	40.2	63.8	43.0	U	44.82
	3×	M	46.5	68.5	50.8	42.1	65.4	45.1		
	3×	C	50.8	69.6	55.1	44.1	67.0	48.1		
Swin-T-PolaFormer	1×	M	44.8	67.6	49.1	40.5	64.1	43.5	U	45.80
	3×	M	47.0	68.9	51.5	42.3	66.0	45.8		
	3×	C	51.1	70.0	55.6	44.4	67.3	48.3		
Swin-T-SAGA	1×	M	45.6(+1.9)	68.0(+1.5)	50.2(+2.5)	41.3(+1.5)	65.0(+1.7)	44.5(+1.8)	U	46.34(+1.83)
	3×	M	47.5(+1.5)	69.1(+1.0)	51.9(+1.6)	42.8(+1.2)	66.0(+0.9)	45.9(+1.0)		
	3×	C	51.5(+1.1)	70.0(+0.8)	55.7(+1.0)	44.9(+1.2)	67.7(+1.1)	48.5(+1.2)		

Table 2: Comparison of object detection and semantic segmentation results on the COCO and ADE20K datasets. In the object detection task, R denotes RetinaNet, M denotes Mask R-CNN, and C denotes Cascade Mask R-CNN. In the semantic segmentation task, S represents Semantic FPN, and U represents UperNet.

and throughput is measured on a single NVIDIA RTX 4090 GPU. Additionally, comprehensive ablation studies are conducted to analyze the effectiveness of the components.

Image Classification

Settings. We trained the model on ImageNet-1K for the classification task, which comprises 1.28M training images and 50K validation images. We selected several widely adopted and representative vision Transformer architectures, including DeiT (Touvron et al., 2021)), PVT (Wang et al., 2021)), PVTv2 (Wang et al., 2022) and Swin Transformer (Liu et al., 2021b), as the baseline models. The self-attention modules in these models are replaced with the proposed attention mechanism to ensure a fair and consistent evaluation across architectures. We employed Top-1 accuracy as the evaluation metric and compared our model with other SOTA models (Yang et al., 2024; Liao et al., 2025; Duan et al., 2024; Huang et al., 2024; Liu et al., 2024, 2022, 2021a). Further setting details are provided in Appendix.

Results. As shown in Tab. 1, our model achieved a significant performance improvement over the baseline model with only a slight increase in FLOPs, thereby demonstrating the superiority of our approach. For instance, Our DeiT-T-SAGA model achieved a 3.3% improvement over the DeiT-T baseline. The PVT-T/S-SAGA models demonstrated enhancements of 4.4% and 2.0% over the PVT-T/S baselines, respectively. Similarly, the Swin-T/S-SAGA models exhibited improvements of 1.7% and 1.7% over the Swin-T/S baselines, respectively. These results indicate that SAGA enriches the feature representation of the KV feature map and can be widely applied to various attention-based models.

Moreover, our model achieves a balance between com-

putational efficiency and performance. Although our model increases the number of FLOPs, it exhibits faster computational speed. For instance, as shown in Tab. 1, the PVT-T-SAGA model has 0.4 more FLOPs than the PVT-T-PolaFormer model, yet its throughput is 472 higher, indicating that SAGA possesses a faster computational speed.

Efficiency Analysis. We visualized the comparison of throughput and peak GPU memory consumption for SAGA, Flatten Attention, Polaformer, and Softmax attention across varying resolutions in Fig. 4 (a) and (b). Specifically, we evaluated the throughput and peak GPU memory consumption of PVT-T-SAGA, PVT-T-Flatten, PVT-T-Polaformer, and PVT-T with varying resolutions. As shown in Fig. 4, while PVT-T has an advantage in throughput at lower resolutions, it runs out of memory when the resolution reaches 1280×1280 , whereas the linear attention mechanism remains unaffected. Compared with PVT-T, our model achieved $1.76\times$ increase in throughput and $2.69\times$ reduction in peak GPU memory consumption when the image resolution is 1280×1280 . Fig. 4 (c) illustrates the trade-off between performance and efficiency of our model. Our model achieves performance improvements while maintaining throughput.

Rank Analysis. To verify whether the proposed KVGate module can increase the rank of the KV feature map and thereby enhance the feature diversity of the semantic repository, we analyzed the rank changes of the KV feature maps for DeiT-T, PVT-T, and Swin-T before and after incorporating the KVGate module. As shown in Fig. 5, before adding KVGate, the rank of the KV feature map in these models often fails to reach full rank and may even decrease with increasing depth of layers. In contrast, after incorporating KV-

Method	Reso	Params	FLOPs	Tp.	Acc(%)
DeiT-T	224 ²	5.7M	1.1G	5761	72.2
EfficientAttn	224 ²	5.7M	1.1G	-	70.2
HydraAttn	224 ²	5.7M	1.1G	-	68.3
EnhancedAttn	224 ²	5.8M	1.1G	-	72.9
FLattenAttn	224 ²	6.1M	1.1G	-	74.1
PolaFormer	224 ²	6.1M	1.2G	-	74.6
SAGA	224²	7.0M	1.4G	4990	75.5
Swin-T	224 ²	28M	4.4G	1511	81.2
HydraAttn	224 ²	29M	4.5G	-	80.7
EfficientAttn	224 ²	29M	4.5G	-	81.0
FLattenAttn	224 ²	29M	4.5G	1397	82.1
PolaFormer	224 ²	29M	4.5G	1205	82.6
SAGA	224²	32M	5.3G	1367	83.0

Table 3: Comparison of various linear attention methods with DeiT and Swin-T on the ImageNet-1K dataset. Tp. (images/s) is measured on a single 4090 GPU with batch size 256.

Gate_Aug	DWC	Output_Aug	Acc.(%)
	✓	✓	82.6(−0.4)
✓	✓		82.3(−0.7)
✓		✓	79.9(−3.1)
✓	✓	✓	83.0

Table 4: Ablation study on each module using Swin-T on ImageNet-1K.

Gate, the rank of the KV feature map essentially reaches full rank, thereby enriching the feature diversity of the semantic repository and enhancing the model’s expressive power.

Object Detection

Settings. We employed PVT-T and Swin-T, both pre-trained with ImageNet-1K weights, as backbones to train the Mask-RCNN (He et al., 2017), RetinaNet (Lin et al., 2017) and Cascade Mask-RCNN (Cai and Vasconcelos, 2019) frameworks on the COCO dataset. Further setting details are provided in Appendix.

Analysis. As shown in Tab. 2 (left), our model achieves superior performance improvements over the original backbone across all frameworks. For instance, when training the Mask R-CNN framework with PVT-T-SAGA and Swin-T-SAGA as backbones using 1x schedule, the models achieved improvements of 3.9% and 1.9% in AP^b over their respective baselines. When training the Cascade Mask R-CNN framework with Swin-T-SAGA as the backbone using a 3x scheduler, the model achieved an improvement of 1.1% in AP^b over the baseline. These results demonstrate that our model can effectively extract task-relevant information from the intermediate SFM while suppressing irrelevant information, thereby enhancing the representational power of the KV feature maps.

Semantic Segmentation

Settings. We employed PVT-T and Swin-T, both pre-trained with ImageNet-1K weights, as backbones to train the SemanticFPN (Kirillov et al., 2019) and UperNet (Xiao et al., 2018) frameworks on the ADE20K dataset. Further setting details are provided in Appendix.

Analysis. As shown in Tab. 2 (right), the Semantic FPN with PVT-T as the backbone achieved a 4.46% improvement in mIoU performance. Meanwhile, the UperNet with Swin-T as the backbone exhibited a 1.83% enhancement in mIoU performance. These results indicate that our model can be widely applied to various model frameworks and can significantly enhance the performance of visual tasks.

Comparison with Other Linear Attention

To demonstrate the advantages of our proposed method over other linear attention modules, we conducted comparative experiments using DeiT and Swin Transformer as baselines. We compared our proposed SAGA with several previous linear attention designs, including efficient attention (Shen et al., 2021), hydra attention (Qin et al., 2022), enhanced attention (Cai, Gan, and Han, 2022), Flatten attention (Han et al., 2023), and Polaformer (Meng et al., 2025b)).

As shown in Tab. 3, our proposed SAGA significantly outperforms the baselines and other linear attention designs. This indicates that the enhancement of the KV feature map can substantially improve the expressive power of linear attention, thereby achieving superior performance with linear complexity.

Ablation Study

As shown in Tab. 4, we evaluated the effectiveness of each component in SAGA. We assessed the impact of introducing a gating mechanism to the intermediate SFM. As shown in row 1 and row 4, the incorporation of the gating mechanism resulted in a 0.4% improvement in performance. This indicates that the information filtering of the intermediate SFM can further enhance the model’s expressive capability.

We also investigated the effect of introducing nonlinearity to the output on performance. By comparing row 2 and row 4, it is evident that the introduction of nonlinearity to the output resulted in a 0.7% improvement in performance. This further underscores the significance of nonlinearity for the ViT-based model.

The comparison between row 3 and row 4 demonstrates that the introduction of local information can enhance the expressive capability of linear attention, thereby improving model performance under linear complexity.

Conclusion

In this work, we introduce SAGA, a novel and efficient linear attention model that incorporates a gating mechanism. By analyzing linear attention through the lens of the semantic repository, we identify the low-rank nature of the KV feature map as the primary cause of performance degradation. Specifically, the KV feature map’s limited capacity to capture distinctions and relationships among all key-value

pairs leads to blurred token information. To mitigate this issue, we propose a gating mechanism that adaptively control the information flow from the SFM to the KV feature map, emphasizing relevant features while suppressing irrelevant ones. Additionally, we propose a Hadamard-product decomposition method to efficiently generate the gating matrix, striking a balance between model efficiency and performance. We validate the effectiveness of SAGA through a series of vision experiments, and the results demonstrate that our method achieves a good trade-off between efficiency and performance. s

References

- Cai, Z., and Vasconcelos, N. 2019. Cascade r-cnn: High quality object detection and instance segmentation. *IEEE transactions on pattern analysis and machine intelligence* 43(5):1483–1498.
- Cai, H.; Gan, C.; and Han, S. 2022. Efficientvit: Enhanced linear attention for high-resolution low-computation visual recognition. *arXiv preprint arXiv:2205.14756* 3.
- Carion, N.; Massa, F.; Synnaeve, G.; Usunier, N.; Kirillov, A.; and Zagoruyko, S. 2020. End-to-end object detection with transformers. In *European conference on computer vision*, 213–229. Springer.
- Chung, J.; Gulcehre, C.; Cho, K.; and Bengio, Y. 2014. Empirical evaluation of gated recurrent neural networks on sequence modeling. *arXiv preprint arXiv:1412.3555*.
- Dai, Z.; Liu, H.; Le, Q. V.; and Tan, M. 2021. Coatnet: Marrying convolution and attention for all data sizes. *Advances in neural information processing systems* 34:3965–3977.
- Deng, J.; Dong, W.; Socher, R.; Li, L.-J.; Li, K.; and Fei-Fei, L. 2009. Imagenet: A large-scale hierarchical image database. In *2009 IEEE conference on computer vision and pattern recognition*, 248–255. Ieee.
- Dosovitskiy, A.; Beyer, L.; Kolesnikov, A.; Weissenborn, D.; Zhai, X.; Unterthiner, T.; Dehghani, M.; Minderer, M.; Heigold, G.; Gelly, S.; et al. 2020. An image is worth 16x16 words: Transformers for image recognition at scale. *arXiv preprint arXiv:2010.11929*.
- Duan, Y.; Wang, W.; Chen, Z.; Zhu, X.; Lu, L.; Lu, T.; Qiao, Y.; Li, H.; Dai, J.; and Wang, W. 2024. Vision-rwkv: Efficient and scalable visual perception with rwkv-like architectures. *arXiv preprint arXiv:2403.02308*.
- Fang, Y.; Yang, S.; Wang, S.; Ge, Y.; Shan, Y.; and Wang, X. 2023. Unleashing vanilla vision transformer with masked image modeling for object detection. In *Proceedings of the IEEE/CVF International Conference on Computer Vision*, 6244–6253.
- Graves, A., and Graves, A. 2012. Long short-term memory. *Supervised sequence labelling with recurrent neural networks* 37–45.
- Han, D.; Pan, X.; Han, Y.; Song, S.; and Huang, G. 2023. Flatten transformer: Vision transformer using focused linear attention. In *Proceedings of the IEEE/CVF international conference on computer vision*, 5961–5971.
- Hassani, A.; Walton, S.; Li, J.; Li, S.; and Shi, H. 2023. Neighborhood attention transformer. In *Proceedings of the IEEE/CVF conference on computer vision and pattern recognition*, 6185–6194.
- He, K.; Gkioxari, G.; Dollár, P.; and Girshick, R. 2017. Mask r-cnn. In *Proceedings of the IEEE international conference on computer vision*, 2961–2969.
- Hou, Q.; Lu, C.-Z.; Cheng, M.-M.; and Feng, J. 2024. Conv2former: A simple transformer-style convnet for visual recognition. *IEEE transactions on pattern analysis and machine intelligence*.
- Huang, T.; Pei, X.; You, S.; Wang, F.; Qian, C.; and Xu, C. 2024. Localmamba: Visual state space model with windowed selective scan. In *European Conference on Computer Vision*, 12–22. Springer.
- Katharopoulos, A.; Vyas, A.; Pappas, N.; and Fleuret, F. 2020. Transformers are rnns: Fast autoregressive transformers with linear attention. In *International conference on machine learning*, 5156–5165. PMLR.
- Kirillov, A.; Girshick, R.; He, K.; and Dollár, P. 2019. Panoptic feature pyramid networks. In *Proceedings of the IEEE/CVF conference on computer vision and pattern recognition*, 6399–6408.
- Liang, J.; Cao, J.; Sun, G.; Zhang, K.; Van Gool, L.; and Timofte, R. 2021. Swinir: Image restoration using swin transformer. In *Proceedings of the IEEE/CVF international conference on computer vision*, 1833–1844.
- Liao, B.; Wang, X.; Zhu, L.; Zhang, Q.; and Huang, C. 2025. Vig: Linear-complexity visual sequence learning with gated linear attention. In *Proceedings of the AAAI Conference on Artificial Intelligence*, volume 39, 5182–5190.
- Lin, T.-Y.; Maire, M.; Belongie, S.; Hays, J.; Perona, P.; Ramanan, D.; Dollár, P.; and Zitnick, C. L. 2014. Microsoft coco: Common objects in context. In *Computer vision—ECCV 2014: 13th European conference, zurich, Switzerland, September 6–12, 2014, proceedings, part v 13*, 740–755. Springer.
- Lin, T.-Y.; Goyal, P.; Girshick, R.; He, K.; and Dollár, P. 2017. Focal loss for dense object detection. In *Proceedings of the IEEE international conference on computer vision*, 2980–2988.
- Liu, H.; Dai, Z.; So, D.; and Le, Q. V. 2021a. Pay attention to mpls. *Advances in neural information processing systems* 34:9204–9215.
- Liu, Z.; Lin, Y.; Cao, Y.; Hu, H.; Wei, Y.; Zhang, Z.; Lin, S.; and Guo, B. 2021b. Swin transformer: Hierarchical vision transformer using shifted windows. In *Proceedings of the IEEE/CVF international conference on computer vision*, 10012–10022.
- Liu, Z.; Mao, H.; Wu, C.-Y.; Feichtenhofer, C.; Darrell, T.; and Xie, S. 2022. A convnet for the 2020s. In *Proceedings of the IEEE/CVF conference on computer vision and pattern recognition*, 11976–11986.

- Liu, Y.; Tian, Y.; Zhao, Y.; Yu, H.; Xie, L.; Wang, Y.; Ye, Q.; Jiao, J.; and Liu, Y. 2024. Vmamba: Visual state space model. *Advances in neural information processing systems* 37:103031–103063.
- Meng, W.; Luo, Y.; Huo, L.; Wang, Y.; Li, X.; and Zhang, Z. 2025a. Nalaformer: Norm-aware linear attention for transformer models. *arXiv preprint arXiv:2506.21137*.
- Meng, W.; Luo, Y.; Li, X.; Jiang, D.; and Zhang, Z. 2025b. Polaformer: Polarity-aware linear attention for vision transformers. *arXiv preprint arXiv:2501.15061*.
- Qin, Z.; Sun, W.; Deng, H.; Li, D.; Wei, Y.; Lv, B.; Yan, J.; Kong, L.; and Zhong, Y. 2022. cosformer: Rethinking softmax in attention. *arXiv preprint arXiv:2202.08791*.
- Shen, Z.; Zhang, M.; Zhao, H.; Yi, S.; and Li, H. 2021. Efficient attention: Attention with linear complexities. In *Proceedings of the IEEE/CVF winter conference on applications of computer vision*, 3531–3539.
- Sun, Y.; Dong, L.; Huang, S.; Ma, S.; Xia, Y.; Xue, J.; Wang, J.; and Wei, F. 2023. Retentive network: A successor to transformer for large language models. *arXiv preprint arXiv:2307.08621*.
- Touvron, H.; Cord, M.; Douze, M.; Massa, F.; Sablayrolles, A.; and Jégou, H. 2021. Training data-efficient image transformers & distillation through attention. In *International conference on machine learning*, 10347–10357. PMLR.
- Wang, W.; Xie, E.; Li, X.; Fan, D.-P.; Song, K.; Liang, D.; Lu, T.; Luo, P.; and Shao, L. 2021. Pyramid vision transformer: A versatile backbone for dense prediction without convolutions. In *Proceedings of the IEEE/CVF international conference on computer vision*, 568–578.
- Wang, W.; Xie, E.; Li, X.; Fan, D.-P.; Song, K.; Liang, D.; Lu, T.; Luo, P.; and Shao, L. 2022. Pvt v2: Improved baselines with pyramid vision transformer. *Computational visual media* 8(3):415–424.
- Xia, Z.; Pan, X.; Song, S.; Li, L. E.; and Huang, G. 2022. Vision transformer with deformable attention. In *Proceedings of the IEEE/CVF conference on computer vision and pattern recognition*, 4794–4803.
- Xiao, T.; Liu, Y.; Zhou, B.; Jiang, Y.; and Sun, J. 2018. Unified perceptual parsing for scene understanding. In *Proceedings of the European conference on computer vision (ECCV)*, 418–434.
- Xie, E.; Wang, W.; Yu, Z.; Anandkumar, A.; Alvarez, J. M.; and Luo, P. 2021. Segformer: Simple and efficient design for semantic segmentation with transformers. *Advances in neural information processing systems* 34:12077–12090.
- Xie, E.; Chen, J.; Chen, J.; Cai, H.; Tang, H.; Lin, Y.; Zhang, Z.; Li, M.; Zhu, L.; Lu, Y.; et al. 2024. Sana: Efficient high-resolution image synthesis with linear diffusion transformers. *arXiv preprint arXiv:2410.10629*.
- Yang, J.; Li, C.; Dai, X.; and Gao, J. 2022. Focal modulation networks. *Advances in Neural Information Processing Systems* 35:4203–4217.
- Yang, S.; Wang, B.; Shen, Y.; Panda, R.; and Kim, Y. 2023. Gated linear attention transformers with hardware-efficient training. *arXiv preprint arXiv:2312.06635*.
- Yang, C.; Chen, Z.; Espinosa, M.; Ericsson, L.; Wang, Z.; Liu, J.; and Crowley, E. J. 2024. Plainmamba: Improving non-hierarchical mamba in visual recognition. *arXiv preprint arXiv:2403.17695*.
- Yuan, Y.; Fu, R.; Huang, L.; Lin, W.; Zhang, C.; Chen, X.; and Wang, J. 2021. Hrformer: High-resolution vision transformer for dense predict. *Advances in neural information processing systems* 34:7281–7293.
- Zhou, B.; Zhao, H.; Puig, X.; Xiao, T.; Fidler, S.; Barriuso, A.; and Torralba, A. 2019. Semantic understanding of scenes through the ade20k dataset. *International Journal of Computer Vision* 127:302–321.